Supplementary Information (SI) for Journal of Materials Chemistry A.
This journal is © The Royal Society of Chemistry 2025

Electronic Supporting Information

Speciation evolution of iron species within ZSM-5 for selective methane oxidation: from redispersion to activation

Xia Chen [a,b], Shuqing Li [a], Lu Bai [c], Jiong Li [d], Yu Fu [a,b,*], Jun Zhang [a,b,*]

[a.] CAS Key Laboratory of Low-Carbon Conversion Science and Engineering, Shanghai Advanced Research Institute, Chinese Academy of Sciences, Shanghai 201210, P.R. China.

[b.] University of the Chinese Academy of Sciences, Beijing 100049, P.R. China

[c.] Western Metal Materials Co., Ltd. Shaanxi, 710201, P.R. China

[d.] Shanghai Synchrotron Radiation Facility, Shanghai Advanced Research Institute, Chinese Academy of Sciences, Shanghai 201210, P.R. China.

[*] Corresponding author.

E-mail addresses: fuy@sari.ac.cn (Y. Fu), zhangj@sari.ac.cn (J. Zhang).

S1. Catalyst preparation

H-ZSM-5 (Si/Al=60) zeolite was obtained from Nankai University Catalyst Co., Ltd. Fe $(NO_3)_3 \cdot 9H_2O$ was purchased from Alfa Aesar. H_2O_2(30%) and D_2O were purchased from Sinopharm Chemical Reagent Co., Ltd. Methanol, and formic acid were obtained from Aladdin. Sodium 3-(trimethylsilyl)-1-propanesulfonate (DSS) was purchased from Tokyo Chemical Industry Co., Ltd.

S2. Catalytic performance evaluation

The specific oxygenates productivity based on per gram catalyst (mmol/g_{cat}), Yield (mmol/(g_{cat}•h)), and oxygenates selectivity (%) were calculated as following equations (1-3):

$$\text{Productivity (mmol/g}_{cat}\text{)} = \frac{\text{n(oxygenated products)}}{g_{cat}} = \frac{\text{n(oxygenated products)}}{g_{cat} \times t} \quad (1)$$

$$\text{Yield (mmol/(g}_{cat}\text{•h))} = \frac{\text{n(oxygenated products)}}{t} \quad (2)$$

$$\text{Oxygenates selectivity (\%)} = \frac{\text{n(oxygenated products)}}{\text{n(total products)}} \times 100\% \quad (3)$$

Where the n(oxygenated products) represented the production of oxygenated products (mmol), n(total products) represented the production of total products including CO_2 (mmol), g_{cat} represented the mass of the catalyst (g), t represented the reaction time (h).

S3. Computational methods.

All the DFT calculations were performed using the quickstep part of the CP2K software.[1, 2] With the framework of the Gaussian plane wave method, CP2K used Gaussian-type orbital functions to represent the Kohn-Sham matrix.[3] An auxiliary plane wave basis was also used to represent the electron density, where the cutoff of the density was 500 Ry. Pseudopotentials of Goedecker, Teter, and Hutter (GTH),[4-6] and MOLOPT basis sets were adopted.[7] To overcome the deficiency of GGA and describe the van der Waals (vdW) interaction accurately, the empirical dispersion van der Waals correction of Grimme's DFT-D3 model was also adopted to describe the weak interaction between FeOx species and zeolite. The energy cutoff was set to be 500 eV. The Brillouin-zone integration was sampled at the Γ-point only due to the large size of the simulation cell. The MFI zeolite has a unit cell of $Si_{96}O_{192}$ containing 12 distinct T sites, which could be substituted by Al partly. The Al pairs was embedded in the intersection of the sine and straight channels of ZSM-5 model in the place of two Si atoms (β-6MR),[8, 9] and a proton was bonded to an adjacent oxygen atom forming the bridging Al-(OH)-Si connection type to balance the charge and consequently generate a Brønsted acid site.

In the construction of the highly dispersed Fe(III) species in Fe-Z5-540N we considered that the average Fe-O coordination in the EXAFS fit is 5.9±0.5 and might eventually be converted α-Fe(IV)=O. By reference to the work of Edward et al.[8] the structure of α-Fe(III)$(O_F)_4$-OH anchored by Al pairs, a macrocyclic ligand similar to the β-6MR of a zeolite, was modeled. The average bond length of Fe-O (2.1 Å) in the optimized models were close to the EXAFS fit (2.02±0.01 Å).In the construction of the highly dispersed Fe(II) site we took into account that the average coordination of Fe-O2 in the EXAFS fit of Fe-Z5-800N is 4.2±0.5, and based on some previously reported structures of α-Fe(II),[10, 11] we therefore constructed α-Fe(II)$(O_F)_4$ that interacts directly with the Al pair, where the average bond length of Fe-O (2.065 Å) is close to that of Fe-O2 (2.06±0.04 Å) in the results of the EXAFS fit.

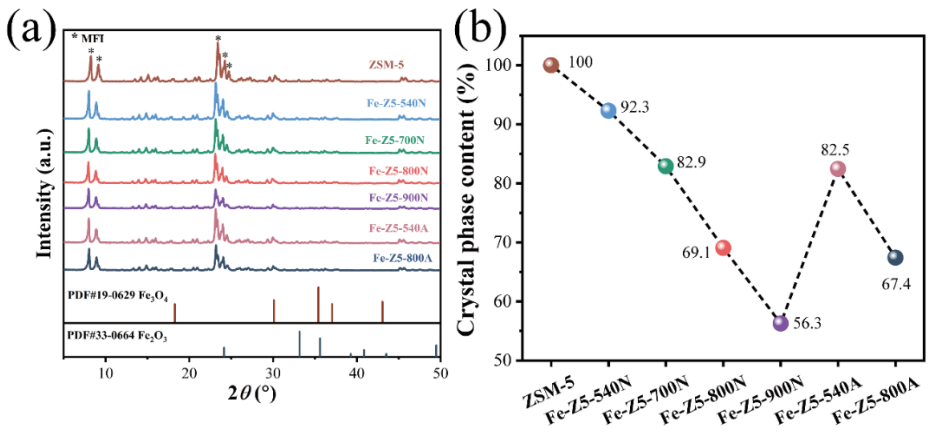

Fig. S1 (a) XRD patterns of catalysts. (b) Crystal phase content of catalysts, ZSM-5 as a reference.

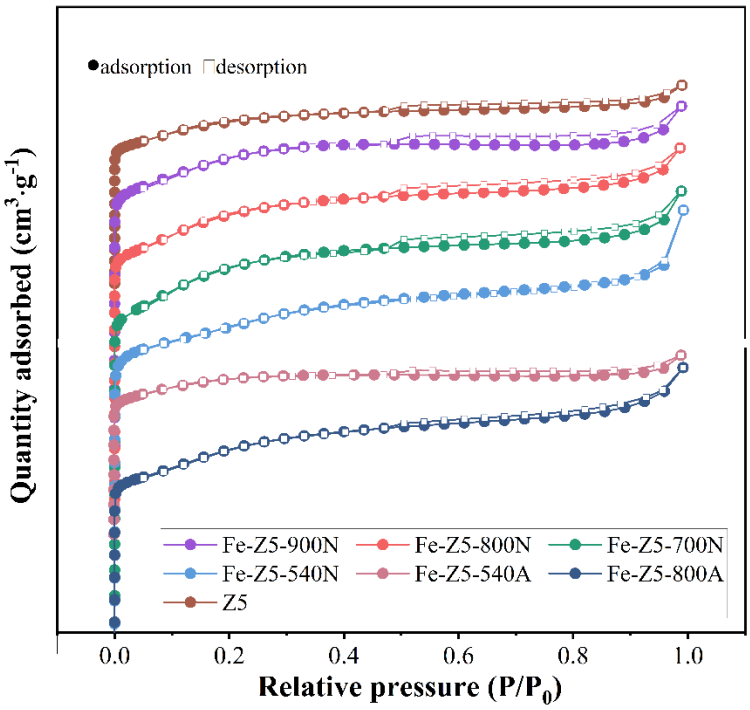

Fig. S2 N_2 adsorption-desorption isotherms of catalysts.

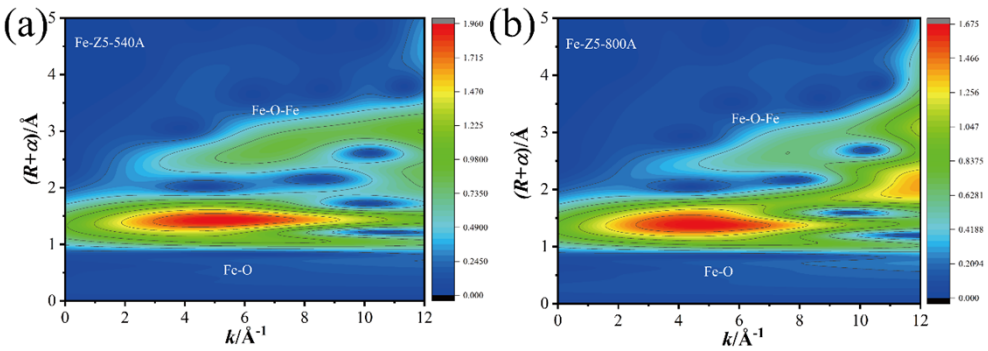

Fig. S3 Wavelet transform spectra. (a)Fe-Z5-540A. (b)Fe-Z5-800A.

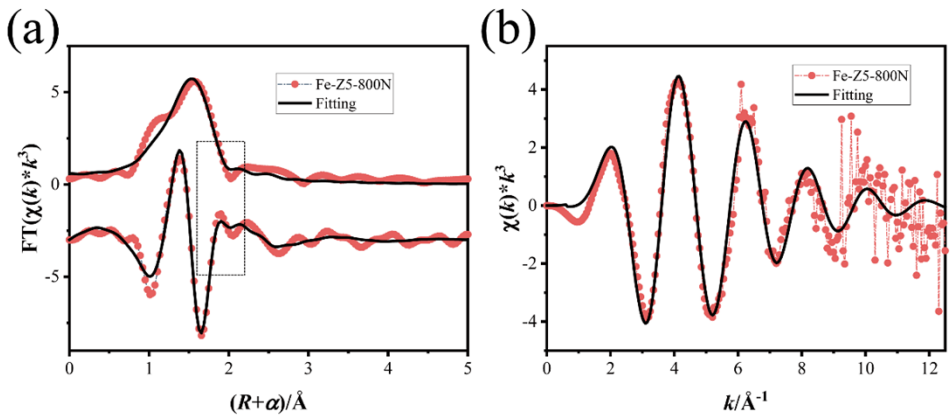

Fig. S4. Fe K-edge EXAFS and curve fit of Fe-Z5-800N using one Fe-O path, show in R-space (FT magnitude and imaginary component) and *k*-space. The data are k^3-weighted and not phase-corrected.

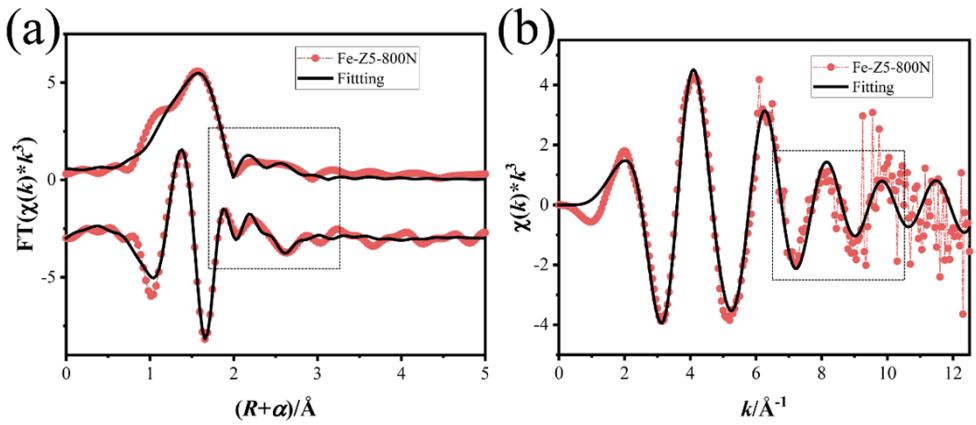

Fig. S5 Fe K-edge EXAFS and curve fit of Fe-Z5-800N using Fe-O1, Fe-O2, and Fe-Fe path, show in R-space (FT magnitude and imaginary component) and *k*-space. The data are k^3-weighted and not phase-corrected.

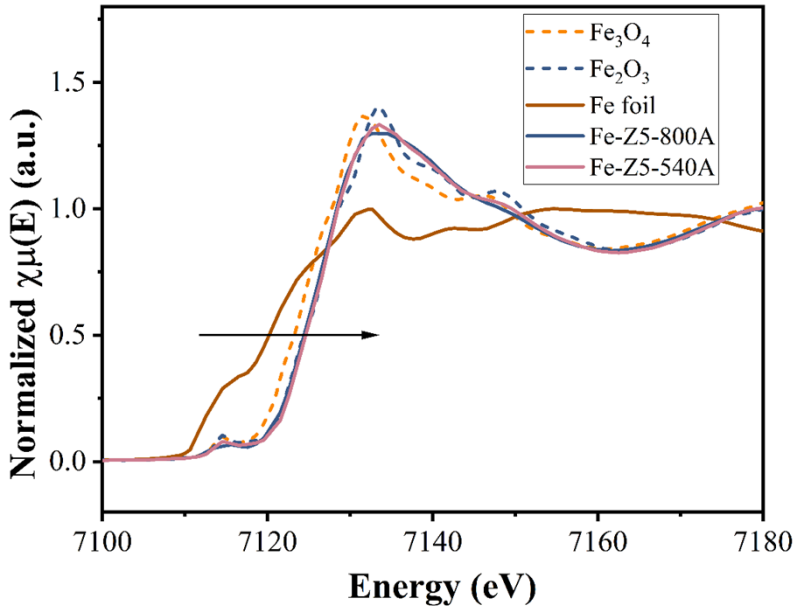

Fig. S6 Fe K-edge XANES spectra of Fe-Z5-540A and Fe-Z5-800A.

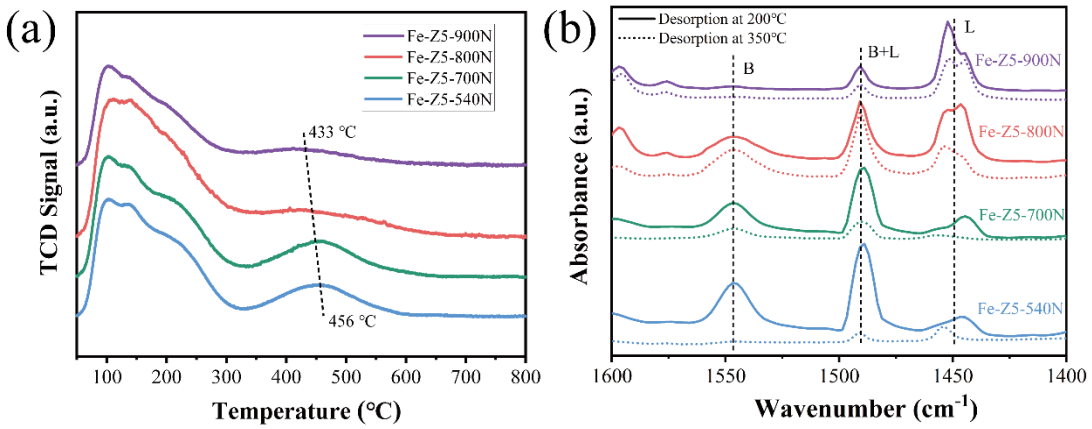

Fig. S7 Acid properties of the catalysts. (a) NH_3-TPD. (b) Py-IR.

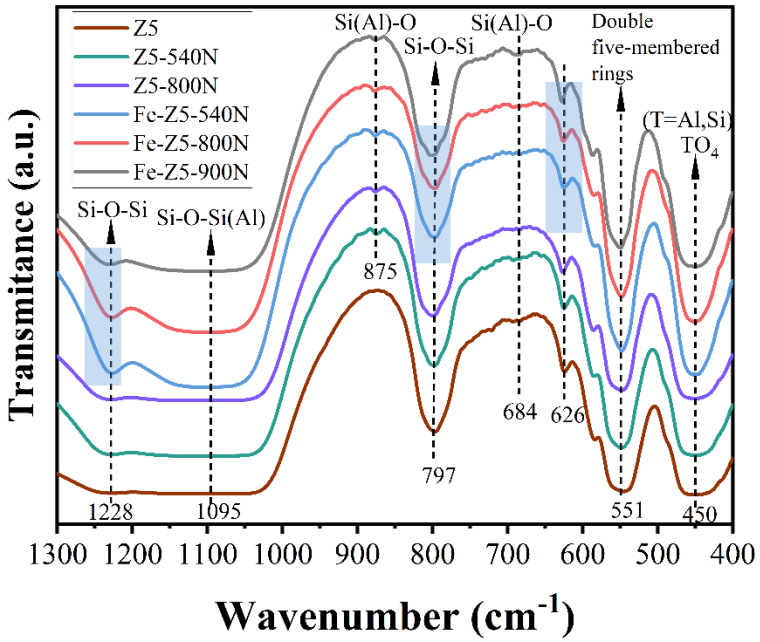

Fig. S8 FTIR spectra of catalysts with different calcination temperatures.

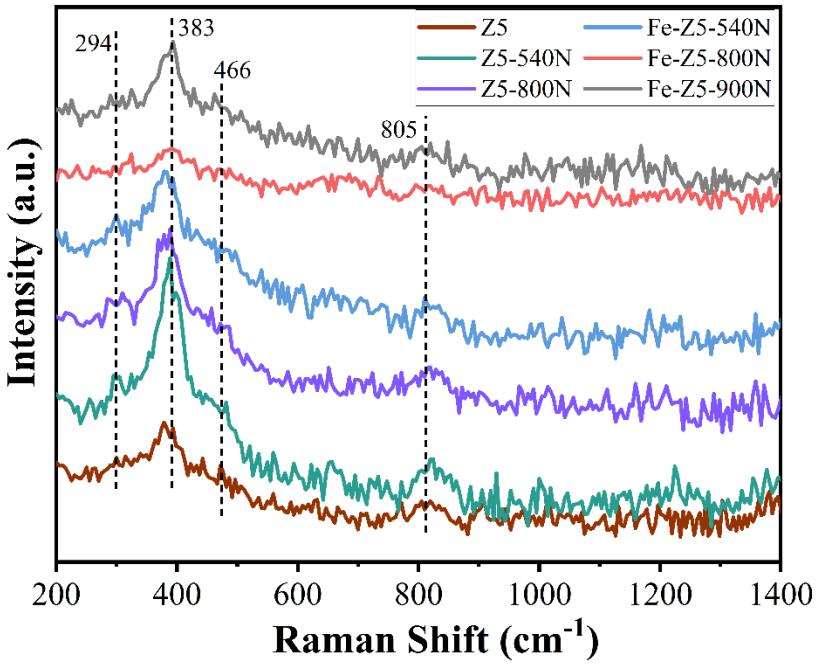

Fig. S9 Raman spectra of catalysts with different calcination temperatures.

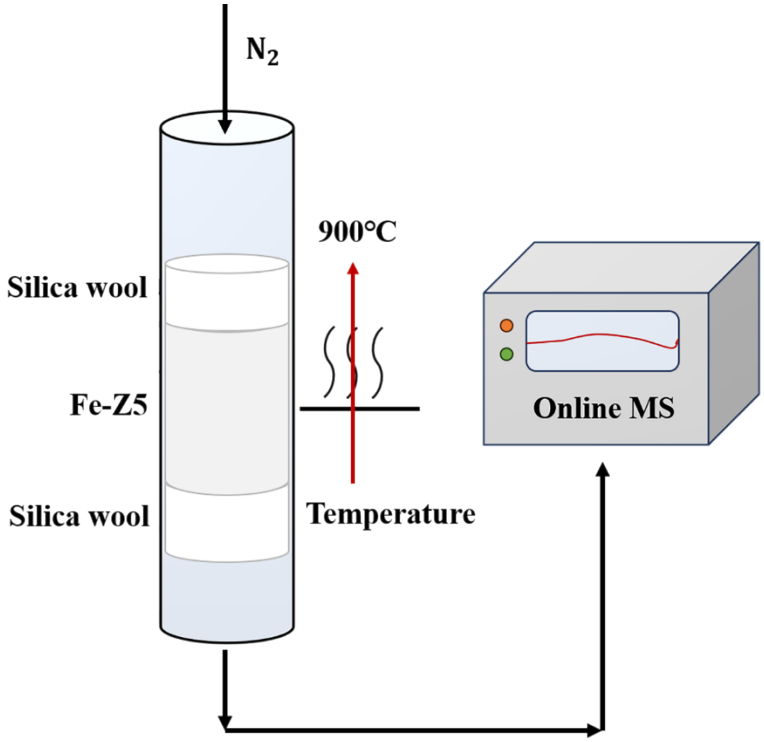

Fig. S10 A direct detection device for the analysis of exhaust during the calcination of Fe-Z5.

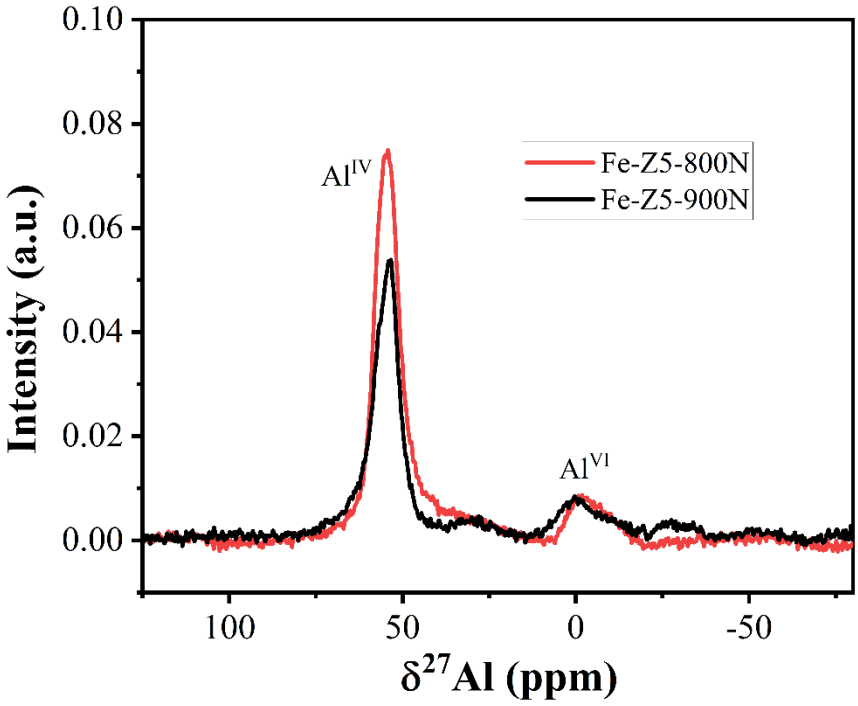

Fig. S11 Single-pulse ^{27}Al MAS NMR of Fe-Z5-800N and Fe-Z5-900N.

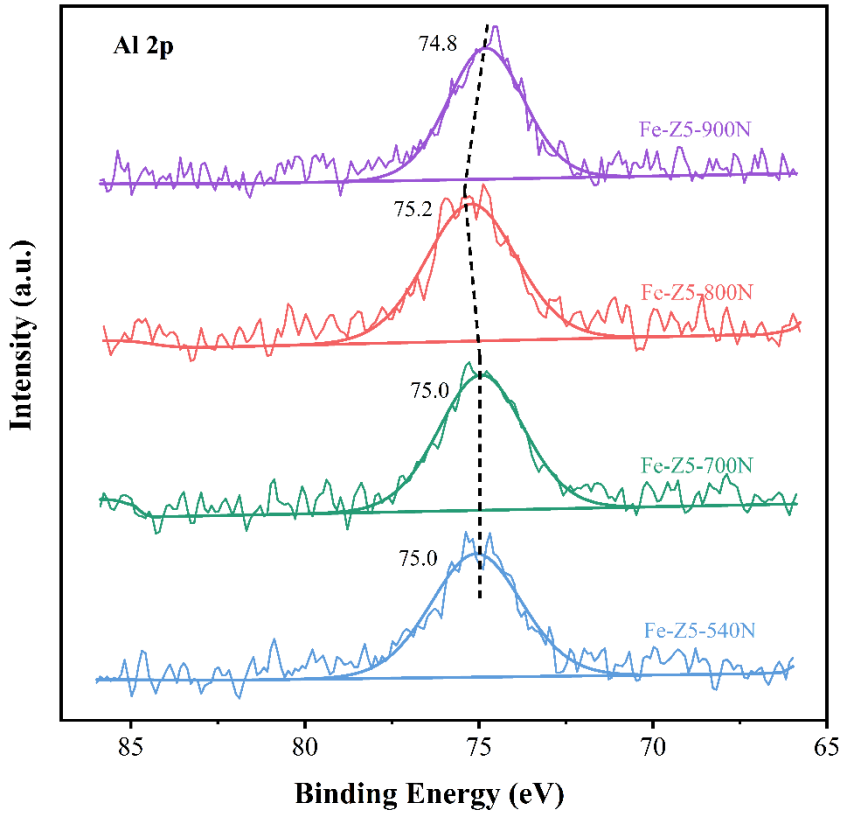

Fig. S12 Al 2p XPS spectra of Fe-Z5 with different calcination temperatures in N_2.

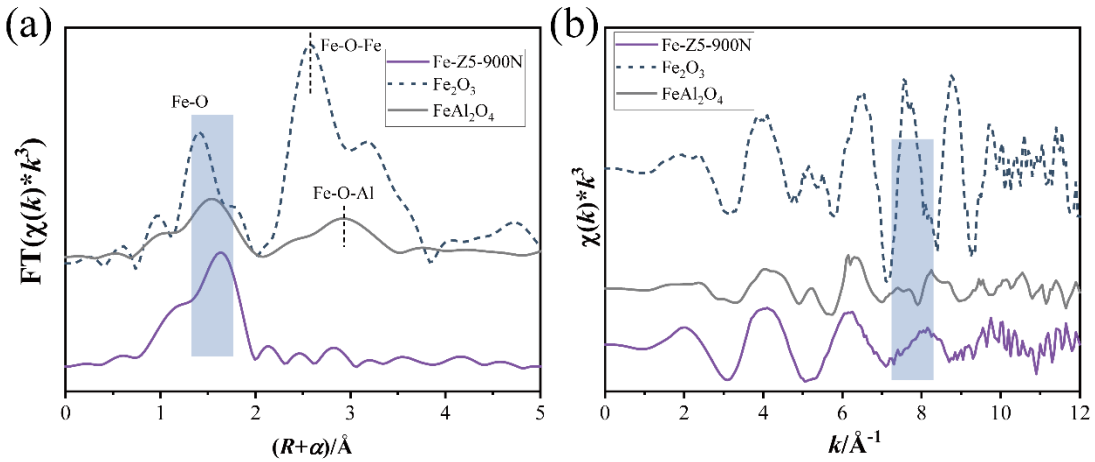

Fig. S13 XAS spectra of Fe species in Fe-Z5. (a) FT-EXAFS spectra, shown in R-space. The data are k^3-weighted and not phase-corrected. (b) FT-EXAFS spectra, shown in *k*-space. The data are k^3-weighted and not phase-corrected.

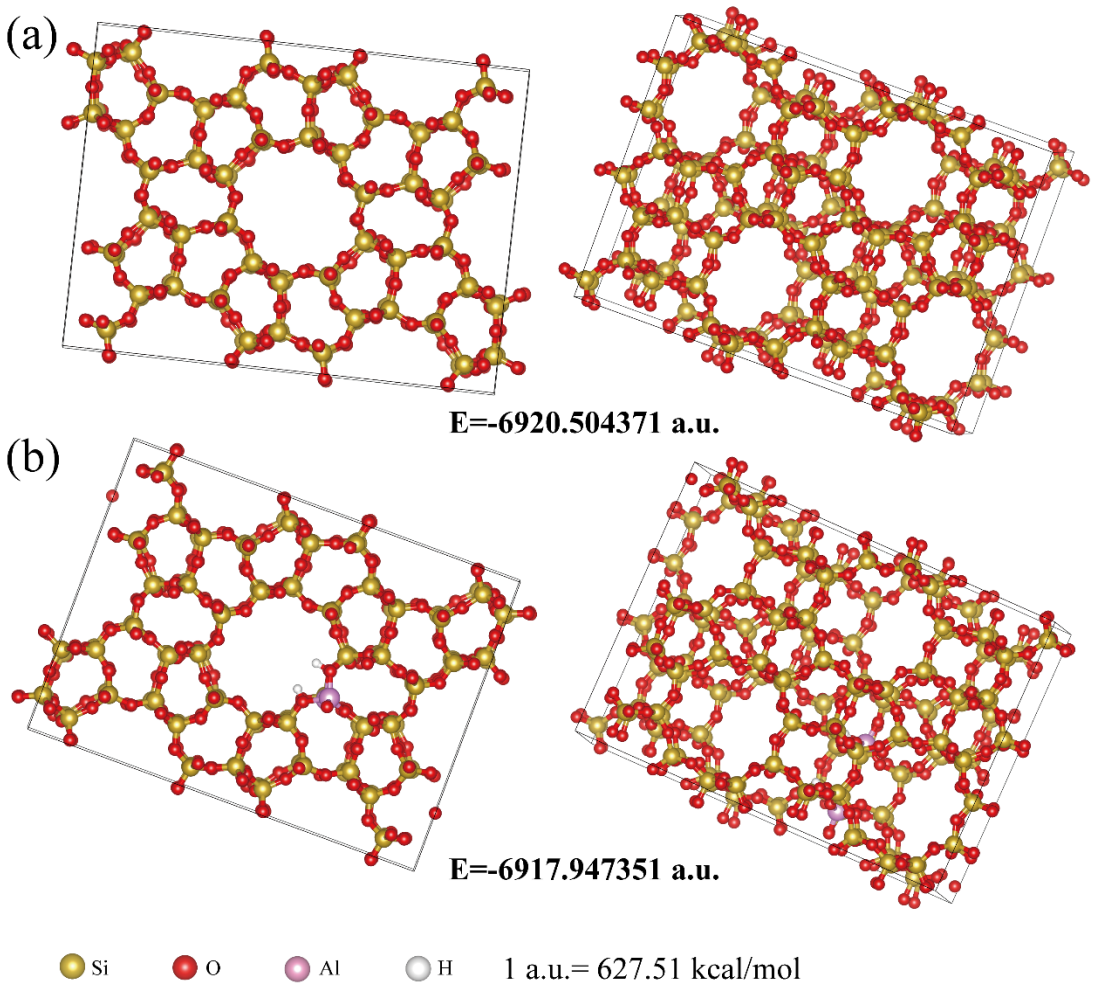

Fig. S14 The model of MFI(a) and 2Al-MFI(b).

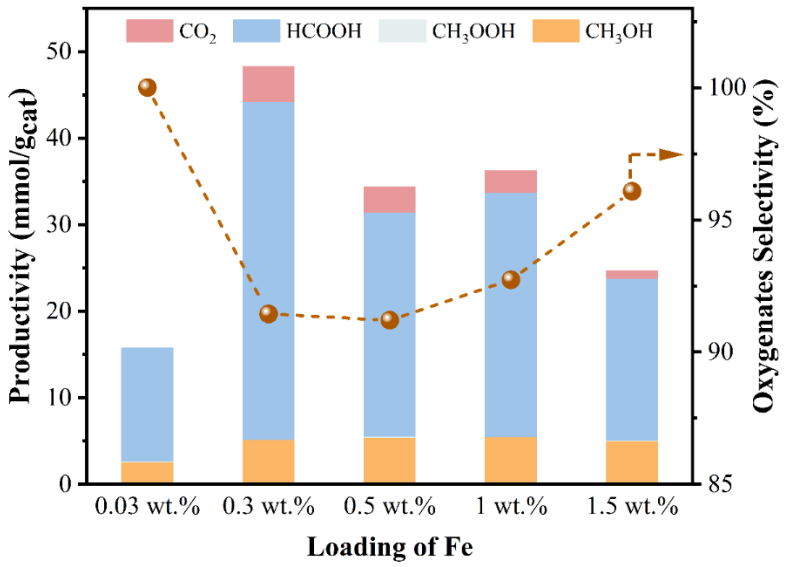

Fig. S15 Catalytic performance of Fe-Z5-800N with different Fe loadings in the same zeolite (Si/Al=60). Reaction condition: 10 mg catalyst, 20 bar CH_4, 10 mL H_2O_2 aqueous solution (0.5M), 1h reaction time, and 50 °C reaction temperature.

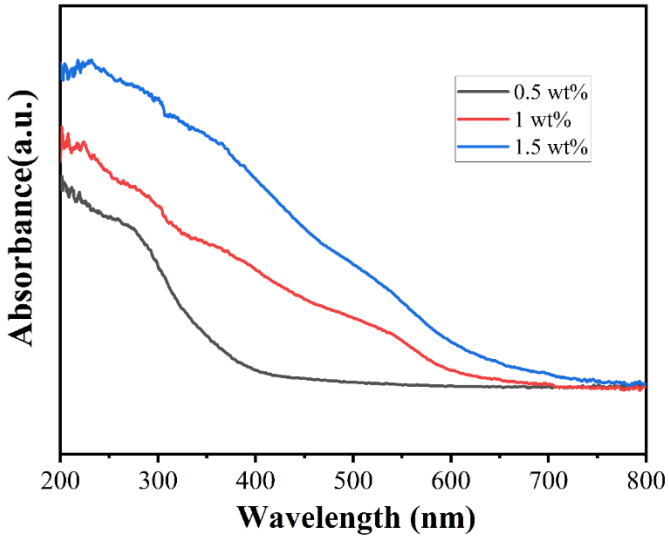

Fig. S16 UV-Vis spectra for different Fe loading.

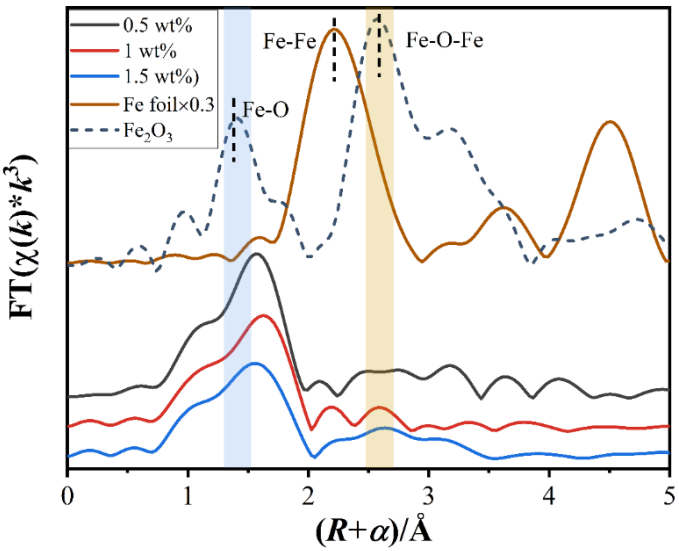

Fig. S17 EXAFS spectra for different Fe loading.

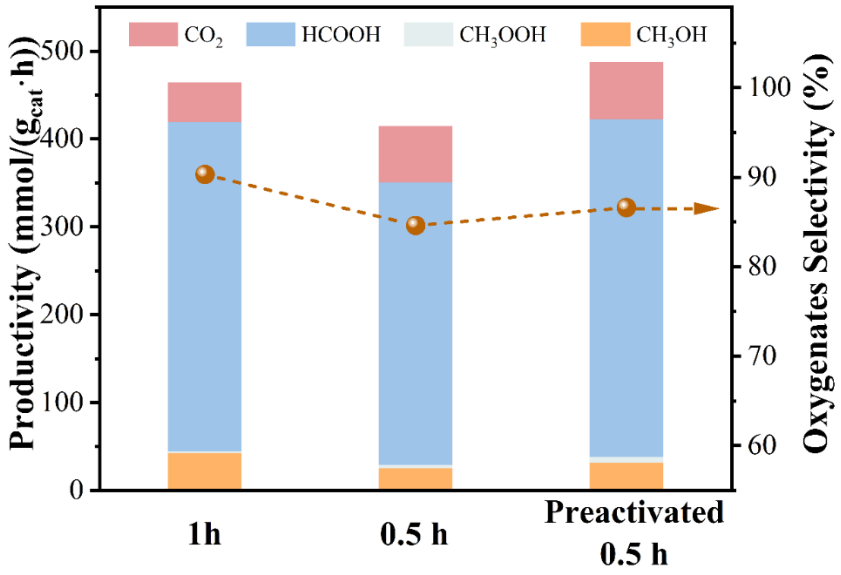

Fig. S18 Catalytic performance of Fe-Z5-800N at 1h, 0.5h and after preactivated 0.5h. Reaction condition: 10 mg catalyst, 20 bar CH_4, 10 mL H_2O_2 aqueous solution (3M), 1h reaction time, and 50 °C reaction temperature.

Table S1. Summary of the textural parameters of catalysts.

Catalysts	Fe loading (wt.%)[a]	Surface area (m^2g^{-1})[b]	Pore volume (cm^3g^{-1})[b]
ZSM	0.04	379.0	0.19
Fe-Z5-540N	0.3	345.3	0.19
Fe-Z5-700N	0.3	343.6	0.18
Fe-Z5-800N	0.31	307.7	0.18
Fe-Z5-900N	0.3	298.6	0.18
Fe-Z5-540A	0.29	302.5	0.17
Fe-Z5-800A	0.29	283.4	0.16

[a] Determined by ICP-OES.

[b] Measured by N_2 physisorption analysis. The surface area was obtained using the Brunauer-Emmett-Teller (BET) method. Pore volume was calculated by the amount of N_2 adsorbed at P/P_0 of 0.99.

Table S2. Fe K-edge EXAFS curve fitting parameters[a]

Sample	Path	R (Å)	CN	σ^2 (Å^2)	ΔE_0 (eV)	R-factor (%)
Fe foil	Fe-Fe1	2.46±0.01	8[b]	0.005±0.001	-1.28±0.01	0.38
	Fe-Fe2	2.84±0.01	6[b]	0.006±0.001		
Fe_2O_3	Fe-O1	1.94±0.02	3[c]	0.003±0.001	0.22±0.01	0.90
	Fe-O2	2.11±0.01	3[c]	0.004±0.001		
	Fe-Fe	2.97±0.07	6[c]	0.007±0.002		
Fe-Z5-900N	Fe-O1[d]	1.93±0.05	5.5±0.6	0.007±0.006	-5.31±0.03	0.67
	Fe-O2[d]	2.00±0.06	2.0±0.7	0.033±0.014		
Fe-Z5-800N	Fe-O1[d]	1.91±0.05	2.1±0.8	0.007±0.002	-0.61±0.03	1.20
	Fe-O2[d]	2.06±0.04	4.2±0.5	0.013±0.016		
Fe-Z5-800N	Fe-O	2.01±0.02	6.5±0.7	0.013±0.002	1.41±0.09	1.80
Fe-Z5-700N	Fe-O	2.00±0.01	6.3±0.6	0.006[e]	-0.33±0.05	0.93
	Fe-Fe	2.99±0.02	2.1±0.1	0.014±0.016		
Fe-Z5-540N	Fe-O	2.02±0.01	5.9±0.5	0.013±0.001	-0.05±0.07	0.85
	Fe-Fe	2.98±0.02	2.4±0.1	0.015±0.016		

[a] R, distance between the absorber and backscatter atoms; CN, coordination number; σ^2, Debye-Waller factor to account for both thermal and structural disorder; ΔE_0, inner potential correction; R-factor indicates the goodness of the fit; S_0^2 was fixed as 0.78 from Fe foil.

[b] This coordination numbers were constrained as CN (Fe-Fe1) =8 and CN (Fe-Fe2) =6 based on the crystal structure of metal Fe.

[c] These coordination numbers were constrained as CN (Fe-O1) =3, CN (Fe-O2) =3 and CN (Fe-Fe) =6 based on the crystal structure of Fe_2O_3.

[d] The distances for the Fe-O1 path were from the crystal structure of the Fe_2O_3 file, and the Fe-O2 path was from the crystal structure of the Al_2FeO_4 file. The fitted paths for the rest of the samples were taken from the crystal structure of the Fe_2O_3 file.

[e] This Debye-Waller factor was constrained as 0.006 for decreasing the correlation.

Table S3. Catalytic performance of various catalysts for methane conversion. [a]

Entry	catalysts	Temperature (°C)	Pressure (bar)	H_2O_2 (mol/L)	CH_3OH (mmol/g_{cat})	CH_3OOH (mmol/g_{cat})	HCOOH (mmol/g_{cat})	CO_2 (mmol/g_{cat})	Yield (mmol/(g_{cat}•h))	Oxygenates Selectivity (%)
1	Z5	50	20	0.5	2.5	0.1	13.2	0	15.8	100
2	Fe-Z5-540A	50	20	0.5	4.5	0.7	27.3	0.9	32.5	97.3
3	Fe-Z5-540N	50	20	0.5	3.6	0	30.3	0.6	33.9	98.3
4	Fe-Z5-700N	50	20	0.5	3.8	0.1	33.8	1.8	37.7	95.4
5	Fe-Z5-800N	50	20	0.5	5.1	0	39.1	4.1	44.2	91.5
6	Fe-Z5-900N	50	20	0.5	3.9	0	31.2	5.2	35.1	87.1
7	Fe-Z5-800A	50	20	0.5	2.3	0.1	10.2	0	12.6	100
8	Fe-Z5-800N	50	20	1.5	38.4	0.8	277.6	19.7	316.8	94.1
9	Fe-Z5-800N	50	20	3	42.5	1.9	374.7	45.0	419.1	90.3
10	Fe-Z5-800N	50	20	5	15.7	1.2	248.9	90.0	265.8	74.7

[a] Reactions conditions note listed: 10 mL H_2O_2, 10 mg catalysts, and 1h reaction time.

Table S4. Comparison of Fe-Z5-800N with various catalysts reported for methane conversion.

Catalysts	H_2O_2 (mol/L)	Pressure /Temperature	Time (h)	Yield (mmol/(g_{cat}•h))	Oxygenates selectivity (%)	Ref
Cu/Fe-ZSM-5	0.5	30.5 bar/50 ºC	0.5	14.02	85	[12]
Fe/ZSM-5	0.277	31 bar/50 ºC	1	17.2	86	[13]
Fe-HZ5-TF	0.5	30.5 bar/75ºC	0.25	109.4	94.3	[14]
Fe-MFI	2.7	30 bar/80 ºC	2	19.4	100	[15]
FeN_4/GN	5	20 bar/25 ºC	10	0.25	94	[16]
MIL-53(Al,Fe)	0.5	30.5 bar/60 ºC	4	5.0	80	[17]
Ag_1-Cu_1/ZSM-5	0.489	30 bar/70 ºC	0.5	46.4	93.4	[18]
Cu_1/ZSM-5	0.51	30 bar/50 ºC	0.5	9.6	99	[19]
Cu_1/ZSM-5	0.51	30 bar/70 ºC	0.5	24.	96	
Cr_1/ZSM-5	0.5-4	30 bar/70 ºC	0.5	21.1	99.8	[20]
Fe-ZIF-8	0.5	30 bar/50 ºC	0.5	2.3	97	[21]
AuPd colloid	0.1	30 bar/50 ºC	0.5	53.6	88	[22]
$CuPdO_2$/CuO	0.5	30 bar/50 ºC	1	4.07	93.9	[23]
Rh_1/ZrO_2	0.5	30 bar/70 ºC	0.5	0.08	78.4	[24]
Cr/TiO_2	0.5 mL H_2O_2 9.5 mL H_2O	30 bar/50 ºC	1	4.4	100	[25]
Ru1/Uio-66	0.5	30 bar/60 ºC	0.25	3.7	~100	[26]
Ce-Uio-Co(OH)	2 mL H_2O_2 8 mL H_2O	30 bar/80 ºC	20	109.5	100	[27]
0.03 wt%Fe/ZSM-5	5	30bar/80 ºC	0.5	421	94	[28]
0.03 wt%Fe/ZSM-5	5	30bar/80 ºC	1	209.3	87.5	
VO-rich TiO_2	0.5 mL H_2O_2 9.5 mL H_2O	30bar/70 ºC	1	1.36	92.5	[29]
Fe-Z5-800N	**3**	**20 bar/50 ºC**	**1**	**419.1**	**90.3**	**This work**

Table S5. The proportion of Fe species at corresponding Fe 2p binding energy over the catalysts with different calcination temperatures.

Sample	Name	Peak BE (eV)[a]	FWHM (eV)[b]	Area (P) CPS.eV[c]	Atomic (%)	Normalized Chi square[d]
Fe-Z5-540N	Fe^{2+} $2p_{3/2}$	709.94	2.88	586.3	26.79	0.306
	Fe^{2+} $2p_{1/2}$	722.74	2.88	303.7		
	Fe^{3+} $2p_{3/2}$	712.07	3.17	1054.27	73.21	
	Fe^{3+} $2p_{1/2}$	725.04	3.17	545.65		
	Fe^{2+} $2p_{3/2}$ satellite peak	714.92	3.37	435.33	/	
	Fe^{3+} $2p_{3/2}$ satellite peak	718.15	3.37	315.74		
	Fe^{2+} $2p_{1/2}$ satellite peak	727.7	3.37	270.05		
	Fe^{3+} $2p_{1/2}$ satellite peak	731.83	3.85	283.45		
Fe-Z5-700N	Fe^{2+} $2p_{3/2}$	710.20	2.94	586.24	30.83	0.412
	Fe^{2+} $2p_{1/2}$	722.74	2.94	303.67		
	Fe^{3+} $2p_{3/2}$	712.37	3.17	865.29	69.17	
	Fe^{3+} $2p_{1/2}$	725.04	3.17	447.84		
	Fe^{2+} $2p_{3/2}$ satellite peak	714.92	3.37	435.33	/	
	Fe^{3+} $2p_{3/2}$ satellite peak	718.15	3.37	315.74		
	Fe^{2+} $2p_{1/2}$ satellite peak	728.08	3.37	250.8		
	Fe^{3+} $2p_{1/2}$ satellite peak	731.89	3.85	237.55		
Fe-Z5-800N	Fe^{2+} $2p_{3/2}$	710.24	2.48	871.43	43.21	0.316
	Fe^{2+} $2p_{1/2}$	723.42	2.48	451.4		
	Fe^{3+} $2p_{3/2}$	712.27	2.69	753.5	56.79	
	Fe^{3+} $2p_{1/2}$	725.56	2.69	389.98		
	Fe^{2+} $2p_{3/2}$ satellite peak	714.89	3.32	627.14	/	
	Fe^{3+} $2p_{3/2}$ satellite peak	717.75	3.27	421.7		
	Fe^{2+} $2p_{1/2}$ satellite peak	728.02	2.96	318.92		
	Fe^{3+} $2p_{1/2}$ satellite peak	731.52	3.37	275.27		
Fe-Z5-900N	Fe^{2+} $2p_{3/2}$	710.04	2.10	141.38	26.28	0.342
	Fe^{2+} $2p_{1/2}$	723.00	2.10	73.23		
	Fe^{3+} $2p_{3/2}$	711.52	2.02	261.01	73.72	
	Fe^{3+} $2p_{1/2}$	724.99	2.01	135.09		
	Fe^{2+} $2p_{3/2}$ satellite peak	713.98	3.08	177.12	/	
	Fe^{3+} $2p_{3/2}$ satellite peak	717.87	3.12	202.69		
	Fe^{2+} $2p_{1/2}$ satellite peak	727.72	2.84	112.5		
	Fe^{3+} $2p_{1/2}$ satellite peak	731.27	2.27	121.94		

[a]Binding Energy (BE): Fe $2p_{1/2}$=Fe $2p_{3/2}$+13.10 (+0.7/-0.3)

[b]Full width at half maxima (FWHM): Fe $2p_{1/2}$=Fe $2p_{3/2}$. Due to the presence of multiple splitting peaks and shock-excitation peaks resulting in broadening of the spectral peaks, the main peak parameter was set in the interval of 0.5:3.5 and the satellite peaks in the interval of 0.5:4.

[c]Area: The ratio of Fe $2p_{1/2}$ to Fe $2p_{3/2}$ is approximately 1/2.

[d]Normalized Chi-square: the difference between the fitted and actual date.

Table S6. Acid properties of the samples.[a]

Catalysts	Acidity amount (mmol/g) [b]			BAS and LAS	
	Weak	Strong	Total	BAS/LAS[c]	BAS/LAS[d]
Fe-Z5-540N	1.49	0.34	1.83	2.04	0.095
Fe-Z5-700N	1.46	0.45	1.91	1.78	1.76
Fe-Z5-800N	1.62	0.42	2.04	0.82	1.47
Fe-Z5-900N	1.00	0.22	1.22	0.048	0.057

[a] The acid amount was obtained directly from the NH_3-TPD test process by instrumental calibration curve and integrating the corresponding desorption peaks. BAS and LAS were obtained from the Py-IR test with the following equations.

$$C_{BAS} = \frac{K_{BAS} \times I_{BAS} \times R^2}{W \times 4} \times 1000$$

$$C_{LAS} = \frac{K_{LAS} \times I_{LAS} \times R^2}{W \times 4} \times 1000$$

$$\frac{BAS}{LAS} = \frac{C_{BAS}}{C_{LAS}}$$

Where the C_{BAS} or C_{LAS} represented the mass of the relative amount of strong BAS or LAS (μmol/g), K_{BAS} or K_{LAS} represented the absorption coefficient of BAS or LAS, 1.88 and 1.42, respectively. I_{BAS} or I_{LAS} represented the peak area of BAS or LAS, R represented the diameter of the tablet, W represented the weight of the tablet (in mg), and R was 1.3 cm.

[b] Determined by NH_3-TPD.

[c] Obtained by Py-IR (200 ºC).

[d] Obtained by Py-IR (350 ºC).

Table S7. Fitting results of ^{27}Al MAS NMR.

Sample		Chemical shifts(ppm)	Peak area	Total peak area	Relative peak area (%)[a]	Relative peak area (%)[b]	Al^{IV}(%)[c]	COD(R^2)[d]
Z5	**Al^{IV}**	48.3	0.16	1.189	13.61	44.15	100	0.9994
		54.3	0.36		30.54			
		56.2	0.61		50.93	55.85		
		62.8	0.059		4.92			
Z5-540N	**Al^{IV}**	49.9	0.071	1.106	6.42	39.87	93.02	0.9995
		54.6	0.37		33.45			
		56.8	0.57		51.54	60.13		
		62.5	0.095		8.59			
Z5-800N	**Al^{V}**	36.2	0.045	0.697	6.46	-	54.84	0.9987
	Al^{IV}	49.6	0.19		27.26	61.69		
		53.3	0.24		34.43			
		56.7	0.16		22.96	31.86		
		60.1	0.062		8.90			
Fe-Z5-540N	**Al^{IV}**	49.4	0.084	1.054	7.96	42.36	88.65	0.9995
		54.6	0.36		34.40			
		56.7	0.42		39.59	57.64		
		60.0	0.19		18.05			
Fe-Z5-800N	**Al^{V}**	37.4	0.040	0.746	5.36	-	59.38	0.9990
	Al^{IV}	48.6	0.13		17.43	65.69		
		53.8	0.36		48.26			
		57.1	0.14		18.77	28.96		
		61.1	0.076		10.19			

[a]The proportions of various peaks were obtained by dividing their deconvolution area by the total area of the signals in the range of 30-70 ppm.

[b]For ZSM-5, the resonance peaks at 45–50 and 53–55 ppm are related to Al located at the intersection channels, respectively, whereas the peaks at 56–60 and 60–65 ppm correspond to Al settled at the straight and/or sinusoidal channel, respectively.

[c]Al^{IV}(%) represents the percentages of Al atoms in the framework, obtained by dividing the total area of the sample at 40-70 ppm by the total area of the Z5 in the range of 40-70 ppm.

[d]COD (coefficient of determination), R^2.

References

1 J. VandeVondele, M. Krack, F. Mohamed, M. Parrinello, T. Chassaing and J. Hutter, *Computer Physics Communications*, 2005, **167**, 103-128.

2 T. D. Kühne, M. Iannuzzi, M. Del Ben, V. V. Rybkin, P. Seewald, F. Stein, T. Laino, R. Z. Khaliullin, O. Schütt, F. Schiffmann, D. Golze, J. Wilhelm, S. Chulkov, M. H. Bani-Hashemian, V. Weber, U. Borštnik, M. Taillefumier, A. S. Jakobovits, A. Lazzaro, H. Pabst, T. Müller, R. Schade, M. Guidon, S. Andermatt, N. Holmberg, G. K. Schenter, A. Hehn, A. Bussy, F. Belleflamme, G. Tabacchi, A. Glöß, M. Lass, I. Bethune, C. J. Mundy, C. Plessl, M. Watkins, J. VandeVondele, M. Krack and J. Hutter, *The Journal of Chemical Physics*, 2020, **152**.

3 J. P. Perdew, K. Burke and M. Ernzerhof, *Phys. Rev. Lett*, 1996, **77**, 3865-3868.

4 S. Goedecker, M. Teter and J. Hutter, *Phys. Rev. B*, 1996, **54**, 1703-1710.

5 C. Hartwigsen, S. Goedecker and J. Hutter, *Phys. Rev. B*, 1998, **58**, 3641-3662.

6 M. Krack, *Theor Chem Acc.*, 2005, **114**, 145-152.

7 J. VandeVondele and J. Hutter, *J. Chem. Phys.*, 2007, **127**.

8 B. E. R. Snyder, P. Vanelderen, M. L. Bols, S. D. Hallaert, L. H. Böttger, L. Ungur, K. Pierloot, R. A. Schoonheydt, B. F. Sels and E. I. Solomon, *Nature*, 2016, **536**, 317-321.

9 Q. Cheng, G. Li, X. Yao, L. Zheng, J. Wang, A. H. Emwas, P. Castano, J. Ruiz-Martinez and Y. Han, *J. Am. Chem. Soc.*, 2023, **145**, 5888-5898.

10 M. L. Bols, S. D. Hallaert, B. E. R. Snyder, J. Devos, D. Plessers, H. M. Rhoda, M. Dusselier, R. A. Schoonheydt, K. Pierloot, E. I. Solomon and B. F. Sels, *J. Am. Chem. Soc.*, 2018, **140**, 12021-12032.

11 M. L. Bols, J. Devos, H. M. Rhoda, D. Plessers, E. I. Solomon, R. A. Schoonheydt, B. F. Sels and M. Dusselier, *J. Am. Chem. Soc.*, 2021, **143**, 16243-16255.

12 C. Hammond, M. M. Forde, M. H. Ab Rahim, A. Thetford, Q. He, R. L. Jenkins, N. Dimitratos, J. A. Lopez-Sanchez, N. F. Dummer, D. M. Murphy, A. F. Carley, S. H. Taylor, D. J. Willock, E. E. Stangland, J. Kang, H. Hagen, C. J. Kiely and G. J. Hutchings, *Angew. Chem. Int. Ed.*, 2012, **51**, 5129-5133.

13 M. S. Kim, K. H. Park, S. J. Cho and E. D. Park, *Catal Today*, 2021, **376**, 113-118.

14 Q. Cheng, G. Li, X. Yao, L. Zheng, J. Wang, A.-H. Emwas, P. Castaño, J. Ruiz-Martínez and Y. Han, *J. Am. Chem. Soc.*, 2023, **145**, 5888-5898.

15 P. Xiao, Y. Wang, T. Nishitoba, J. N. Kondo and T. Yokoi, *ChemComm.*, 2019, **55**, 2896-2899.

16 X. Cui, H. Li, Y. Wang, Y. Hu, L. Hua, H. Li, X. Han, Q. Liu, F. Yang, L. He, X. Chen, Q. Li, J. Xiao, D. Deng and X. Bao, *Chem*, 2018, **4**, 1902-1910.

17 D. Y. Osadchii, A. I. Olivos-Suarez, Á. Szécsényi, G. Li, M. A. Nasalevich, I. A. Dugulan, P. S. Crespo, E. J. M. Hensen, S. L. Veber, M. V. Fedin, G. Sankar, E. A. Pidko and J. Gascon, *ACS Catal.*, 2018, **8**, 5542-5548.

18 B. Y. Yu, L. Cheng, S. Dai, Y. J. Jiang, B. Yang, H. Li, Y. Zhao, J. Xu, Y. Zhang, C. S. Pan, X. M. Cao, Y. F. Zhu and Y. Lou, *Adv. Sci.*, 2023, **10**, 2302143.

19 X. Tang, L. Wang, B. Yang, C. Fei, T. Yao, W. Liu, Y. Lou, Q. Dai, Y. Cai, X.-M. Cao, W. Zhan, Y. Guo, X.-Q. Gong and Y. Guo, *Appl. Catal. B Environ. Energy*, 2021, **285**, 119827.

20 M. Zeng, L. Cheng, Q. Gu, B. Yang, B. Yu, J. Xu, Y. Zhang, C. Pan, X.-M. Cao, Y. Lou and Y. Zhu, *EES Catal*, 2023, **1**, 153-161.

21 L. Lin, G. Zhang, L. Kang, T. Yu, Y. Su, G. Zeng, S. Chu and W. Luo, *ChemCatChem*, 2023, **15**, e202201234.

22 N. Agarwal, S. J. Freakley, R. U. McVicker, S. M. Althahban, N. Dimitratos, Q. He, D. J. Morgan, R. L. Jenkins, D. J. Willock, S. H. Taylor, C. J. Kiely and G. J. Hutchings, *Science*, 2017, **358**, 223-227.

23 S. Bai, Y. Xu, P. Wang, Q. Shao and X. Huang, *ACS Catal.*, 2019, **9**, 6938-6944.

24 Y. Kwon, T. Y. Kim, G. Kwon, J. Yi and H. Lee, *J. Am. Chem. Soc.*, 2017, **139**, 17694-17699.

25 Q. Shen, C. Cao, R. Huang, L. Zhu, X. Zhou, Q. Zhang, L. Gu and W. Song, *Angew. Chem. Int. Ed.*, 2019, **59**, 1216-1219.

26 G. Fang, F. Wei, J. Lin, Y. Zhou, L. Sun, X. Shang, S. Lin and X. Wang, *J. Am. Chem. Soc*, 2023, **145**, 13169-13180.

27 N. Antil, M. Chauhan, N. Akhtar, R. Newar, W. Begum, J. Malik and K. Manna, *ACS Catal.*, 2022, **12**, 11159-11168.

28 K. Zhu, S. Liang, X. Cui, R. Huang, N. Wan, L. Hua, H. Li, H. Chen, Z. Zhao, G. Hou, M. Li, Q. Jiang, L. Yu and D. Deng, *Nano Energy*, 2021, **82**,105718.

29 H. Yin, Z. Pu, J. Xue, P. Ma, B. Wu, M. Han, H. Lin, Z. Luo, J. Zeng, X. Ma and H. Li, *ACS Catal.*, 2023, **13**, 7608-7615.